Substantially positive contributions of new particle formation to Cloud Condensation Nuclei under low supersaturation in China based on numerical model improvements

Chupeng Zhang[1#], Shangfei Hai[2,11#], Yang Gao[1*], Yuhang Wang[3*], Shaoqing Zhang[4,2], Lifang Sheng[2], Bin Zhao[5], Shuxiao Wang[5], Jingkun Jiang[5], Xin Huang[6], Shen Xiaojing[7], Sun Junying[7], Aura ~~Lupascu[7]~~Lupascu[8], Manish ~~Shrivastava[8]~~Shrivastava[9], Jerome D. ~~Fast[8]~~Fast[9], Wenxuan Cheng[1], Xiuwen Guo[1], Ming Chu[1], Nan ~~Ma[9]~~Ma[10], Juan ~~Hong[9]~~Hong[10], Qiaoqiao ~~Wang[9]~~Wang[10], Xiaohong Yao[1] and Huiwang Gao[1]

[1]Frontiers Science Center for Deep Ocean Multispheres and Earth System, and Key Laboratory of Marine Environmental Science and Ecology, Ministry of Education, Ocean University of China, and Laoshan Laboratory, Qingdao, 266100, China

[2]College of Oceanic and Atmospheric Sciences, Ocean University of China, Qingdao, 266100, China

[3]School of Earth and Atmospheric Sciences, Georgia Institute of Technology, Atlanta, GA, 30332, USA

[4]Frontiers Science Center for Deep Ocean Multispheres and Earth System, and Key Laboratory of Physical Oceanography, Ocean University of China, and Laoshan Laboratory, Qingdao, 266100, China

[5]State Key Joint Laboratory of Environment Simulation and Pollution Control, School of Environment, Tsinghua University, Beijing, 100084 China， and State Environmental Protection Key Laboratory of Sources and Control of Air Pollution Complex, Beijing 100084, China

[6]School of Atmospheric Sciences, Nanjing University, Nanjing, 210023, China

[7]~~Institute~~State Key Laboratory of Severe Weather & Key Laboratory of Atmospheric Chemistry of CMA, Chinese Academy of Meteorological Sciences, Beijing, 100081, China

[8]Institute for Advanced Sustainability Studies, Potsdam D-14467, Germany

[8]~~Atmospheric~~[9]Atmospheric Sciences and Global Change Division, Pacific Northwest National Laboratory, Richland, WA, 99354, USA

[9]~~Institute~~[10]Institute for Environmental and Climate Research, Jinan University, Guangzhou, 510000, China

[11]CMA Earth System Modeling and Prediction Center, China Meteorological Administration, Beijing 100081, China

[#]Authors contributed equally to this study.

[*]To whom correspondence to: yanggao@ouc.edu.cn, yuhang.wang@eas.gatech.edu

Abstract

New particle formation (NPF) and subsequent particle growth are important sources of condensation nuclei (CN) and cloud condensation nuclei (CCN). While ~~a number of~~many observations have shown positive contributions of NPF to CCN at low supersaturation, negative NPF contributions were often simulated~~.~~ in polluted environment. Using the observations in a typical coastal city of Qingdao, we thoroughly evaluate the simulated number concentrations of CN and CCN using a NPF-explicit parameterization embedded in WRF-Chem model. In terms of CN, the initial simulation shows large biases of particle number concentrations at 10–40 nm ($CN_{10–40}$) and 40–100 nm ($CN_{40–100}$). By adjusting the process of gas-particle partitioning, including mass accommodation coefficient of sulfuric acid, the phase changes of primary organic aerosol emissions and the condensational amount of nitric acid, the concomitant improvement of the particle growth process yields a substantial reduction of overestimates of $CN_{10–40}$ and $CN_{40–100}$. Regarding CCN, SOA formed from the oxidation of semi-volatile and intermediate volatility organic vapors (SI-SOA) yield is an important contributor. In the original WRF-Chem model with 20 size bins setting, the yield of SI-SOA is too high without considering the differences in oxidation rates of the precursors. Lowering the SI-SOA yield results in much improved simulations of the observed CCN concentrations. On the basis of the bias-corrected model, we find substantial positive contributions of NPF to CCN at low supersaturation (~0.2%) in Qingdao and over the broad areas of China, primarily due to the competing effects of increasing particle hygroscopicity surpassing that of particle size decrease. This study highlights the potentially much larger NPF contributions to CCN on a regional and even global basis.

1. Introduction

New particle formation (NPF) is a process in which gaseous vapors nucleate and form critical molecular clusters, followed by subsequent growth to larger sizes through condensation and coagulation ~~(Kulmala et al., 2004; Kulmala et al., 2013; Lee et al., 2019)~~(Kulmala et al., 2004; Kulmala et al., 2013; Lee et al., 2019). Newly formed particles could effectively grow into the size of cloud condensation nuclei (CCN) under certain supersaturation (SS), which exerts an impact on the cloud microphysical process and global radiation balance ~~(Merikanto et al., 2009; Gordon et al., 2017; Kerminen et al., 2018; Ren et al., 2021)~~(Merikanto et al., 2009; Gordon et al., 2017; Kerminen et al., 2018; Ren et al., 2021). In addition, the ~~high-efficiency~~efficient nucleation and explosive growth of particles may contribute to the formation of haze ~~(Guo et al., 2014)~~(Guo et al., 2014), affecting air quality and human health (~~Yuan et al., 2015~~Yuan et al., 2015; ~~Chu et al., 2019~~Chu et al., 2019; Kulmala et al., 2021).

The overestimate of condensation nuclei (CN) in numerical models are commonly seen, despite the attempt to ~~correctify~~rectify the bias ~~(Matsui et al., 2013~~(Matsui et al., 2013; Arghavani et al., 2022). It is a common way to reduce the nucleation rate which may reduce the particle number concentration in proportion ~~(Matsui et al., 2013)~~(Matsui et al., 2013). For instance, in the study of NPF in East Asia in the spring of 2009, even after lowering the nucleation rate in a regional model of WRF-Chem applied in their study, the reduced number concentration of particles at 10–130 nm remained to be overestimated ~~(Matsui et al., 2013)~~(Matsui et al., 2013). Using the same regional model and a similar method to reduce the nucleation rate, Arghavani et al. (2022) found particle number concentration at 10–100 nm was still overestimated by nearly one order of magnitude, despite the effectiveness to reduce the overestimates for the smaller particles such as 2.5–10 nm. In addition to the rate of NPF, the growth

process of particles also has a crucial effect on particle number concentration and size distribution. In this process, the condensation of some chemical species such as sulfuric acid, nitrate and organic gases on particles plays a major role in particle growth ~~(Yao et al., 2018; Lee et al., 2019; Li et al., 2022)~~(Yao et al., 2018; Lee et al., 2019; Li et al., 2022), and the uncertainty of their condensation amount may lead to the bias of CN simulation.

In addition to CN, there are large discrepancies in the predicted CCN between the numerical models and observational results. Furthermore, as an important source of CCN ~~(Merikanto et al., 2009)~~(Merikanto et al., 2009), the contribution of nucleation to CCN quantified by numerical models is also highly uncertain. For example, in terms of predicting CCN, ~~Fanourgakis et al. (2019)~~Fanourgakis et al. (2019) evaluated the CCN concentrations simulated by 16 global aerosol–climate and chemistry transport models with observations at 9 sites in Europe and Japan from 2011 to 2015, and found that all models underestimated CCN concentrations with a mean normalized mean bias ~~(NMB)~~ of -36% at low supersaturation (SS=0.2%). ~~Models~~WRF-Chem models also tend to underestimate the contribution of NPF on CCN, especially at low supersaturation. The continuous observation of CCN concentrations throughout the year (July 2008–June 2009) carried out in Hyytiälä, Finland, showed that under low SS, nucleation enhanced the CCN by 106% and 110% at SS=0.1% and 0.2% respectively ~~(Sihto et al., 2011)~~(Sihto et al., 2011). Observations acquired in Beijing from July 12 to September 25, 2008, also suggested that nucleation significantly increases CCN at all supersaturations, even when supersaturation is low (i.e., 0.07% and 0.26%). Thus, the occurrence of NPF enhanced CCN by a factor of 1.7 and 2.2, respectively ~~(Yue et al., 2011)~~(Yue et al., 2011).

However, previous numerical experiments behave oppositely. ~~For instance, Matsui et al. (2011) quantified the contribution of nucleation to CCN using WRF-chem in Beijing in August and September 2006 and found reduced CCN under low SS, e.g., when SS=0.02%, the concentration of CCN is reduced by up to ~50%. They attributed this to the fact that the small particles produced by nucleation may inhibit the growth of the preexisting particles~~ For instance, Matsui et al. (2011) quantified the contribution

of nucleation to CCN using WRF-chem in Beijing in August and September 2006 and found reduced CCN under low SS, e.g., when SS=0.02%, the concentration of CCN is reduced by up to ~50%. They attributed this to the fact that the small particles produced by nucleation may inhibit the growth of the preexisting particles ~~(Matsui et al., 2011)~~(Matsui et al., 2011). Similarly, ~~Dong et al. (2019)~~Dong et al. (2019) conducted NPF simulations with the WRF-Chem for the summer of 2008 focusing on the Midwest of the United States, and found that the nucleation resulted in decreased CCN at low supersaturation (SS=0.1%). Besides, a study carried out for East Asia in 2009 also indicated that at low supersaturation (e.g. SS=0.1%), nucleation has little impact on CCN ~~(Matsui et al., 2013)~~(Matsui et al., 2013). The contrasting effects of nucleation on CCN at low supersaturations in model and observations is not explained in these previous studies.

At the stage of particle growth, secondary organic aerosol (SOA) formed by atmospheric oxidation of organic vapors is a major contributor to particle growth to CCN-related sizes ~~(Liu and Matsui, 2022; Qiao et al., 2021)~~(Liu and Matsui, 2022; Qiao et al., 2021). SOA formed by multi-generational gas-phase oxidation of semi-volatile and intermediate volatility organic compounds (S/IVOC) is called SI-SOA ~~(Jimenez et al., 2009; Zhang et al., 2007)~~(Jimenez et al., 2009; Zhang et al., 2007)~~. Zhao et al. (2016)~~. Zhao et al. (2016) made a comprehensive assessment of the roles of various SOA precursors in SOA formation in real atmosphere in China in 2010, and the results demonstrated that evaporated POA and IVOC (i.e. S/IVOC) made a significant contribution to SOA, contributing up to 82% to the average SOA concentration in eastern China. However, the effect of SI-SOA on CCN has not been fully studied.

In this paper, WRF-Chem was applied to simulate the effect of the NPF on CCN in Qingdao in February 2017. The simulated results from the WRF-Chem model are firstly compared with observations in Qingdao, exhibiting large biases in CN. This is followed by an improvement through a few processes. At the end, the impact of SI-SOA yield and nucleation on CCN is investigated.

2. Data and methods

2.1 Observations

The measurements used in this study were carried out over the sampling site from February 5 to 24, 2017 at the campus of Ocean University of China (36°09′37″N, 120°29′44″E) in Qingdao, which is surrounded by residential buildings and is situated about 10 km away from the city center. A fast mobility particle sizer (FMPS, TSI Model 3091) was applied to measure the aerosol particle size distribution for the size range of 5.6 nm to 560 nm ~~(Liu et al., 2014b)~~(Liu et al., 2014b)~~. The size-resolved CCN activity is measured by a cloud condensation nuclei counter (CCNc) at three different supersaturations (0.2%, 0.4% and 0.6%) and each supersaturation lasts for 5 minutes. More information about the CCN measurement can be found in Li et al. (2015).~~. The bulk CCN concentration is measured by a cloud condensation nuclei counter at three different supersaturations (0.2%, 0.4% and 0.6%) and each supersaturation lasts for 20 minutes. More information about the CCN measurement can be found in Li et al. (2015). The urban site in Beijing is located on the roof of the building of the Chinese Academy of Meteorological Sciences (CAMS, 39°95′N, 116°33′E) in the campus of the China Meteorological Administration, close to the main road with heavy traffic. The rural site is Gucheng (GC, 39°08′N, 115°40′E), located in Hebei Province, surrounded by farmland, and is a representative station of the severity of air pollution in Beijing Tianjin Hebei region. The particle number size distribution of these two sites in the range of 4–850 nm is measured by a Tandem Scanning Mobility Particle Sizer (TSMPS), and more information about the instruments can be found in Shen et al. (2018).

2.2 Model configurations

WRF-Chem version 3.9 is used to simulate NPF events, with the main physical and chemical parameterization settings summarized in Table 1. The spatial resolution is 36 km by 36 km with 35 vertical layers and a model top at 50 hPa. The regional model simulations at a higher spatial resolution may be desirable in future when urban pollution is focused. A continuous run from February 1 to 25, 2017, was conducted, with the first five-day results as the spin-up and discarded in the analysis.

Table 1 WRF-Chem model configurations used in this work

	Model configuration
Microphysics	Morrison 2-moment microphysics scheme ~~(Morrison et al., 2009)~~(Morrison et al., 2009)
Planetary Boundary Layer (PBL)	YSU boundary layer scheme ~~(Hong et al., 2006)~~(Hong et al., 2006)
Longwave and Shortwave Radiation	RRTMG longwave and shortwave radiation ~~(Iacono et al., 2008)~~(Iacono et al., 2008)
Land model	Unified Noah Land Surface scheme ~~(Chen and Dudhia, 2000; Tewari et al., 2016)~~(Chen and Dudhia, 2000; Tewari et al., 2016)
Cumulus	Grell-3D cumulus parameterization scheme ~~(Grell, 1993)~~(Grell, 1993)
Aerosol module	MOSAIC module ~~(Zaveri et al., 2008; Matsui et al., 2011)~~(Zaveri et al., 2008; Matsui et al., 2011)
Gas-phase Chemistry	SAPRC-99 gas-phase chemistry scheme ~~(Carter, 2000)~~(Carter, 2000)

The meteorological initial and boundary conditions are driven by Climate Forecast System model version 2 (CFSv2; ~~(Saha et al., 2014)~~(Saha et al., 2014)) reanalysis developed by National Centre for Environmental Prediction (NCEP). The initial and boundary chemical conditions of WRF-Chem are provided by Community Atmosphere Model with Chemistry (CAM-Chem; ~~(Buchholz et al., 2019)~~(Buchholz et al., 2019)). Anthropogenic emissions for the year of 2017 are obtained from the Multiresolution Emission Inventory for China (MEIC, http://www.meicmodel.org/) emission dataset ~~(Li et al., 2017; Zheng et al., 2018)~~(Li et al., 2017; Zheng et al., 2018).

The Model for Simulating Aerosol Interactions and Chemistry (MOSAIC) was used to delineate dynamic gas-particle mass transfer to represent the condensation growth of aerosol ~~(Zaveri et al., 2008)~~(Zaveri et al., 2008). The gas-particle partitioning of gas species on particles is regulated by the mass transfer rate, which is related to mass accommodation coefficient (α), a parameter involved in the model representing

the probability of gas molecules entering the bulk liquid phase ~~(Pöschl et al., 1998)~~(Pöschl et al., 1998). The original setting of α for all condensing species for all size bins a in MOSAIC is 0.1 ~~(Zaveri et al., 2008)~~(Zaveri et al., 2008). In the default release of WRF-Chem, MOSAIC was implemented in the sectional framework with aerosol size distributions divided into 4 or 8 size bins spanning 39 nm to 10 μm in diameter. To explicitly express the nucleation and the growth of newly formed particles, the aerosol size range in the MOSAIC module was extended from 1 nm to 10 μm, with the number of aerosol size bins increased to 20 ~~(Matsui et al., 2011; Matsui et al., 2013; Lupascu et al., 2015; Lai et al., 2022)~~(Matsui et al., 2011; Matsui et al., 2013; Lupascu et al., 2015; Lai et al., 2022)~~.~~. The calculation method of CCN concentration in the WRF-chem model is referred to the study of Matsui et al. (2011). Based on Köhler theory, CCN concentrations under the three given supersaturations of 0.2%, 0.4% and 0.6% were calculated. The critical supersaturation (S_c) of each size bin in the WRF-chem model was calculated by the following formula:

$$S_c = \sqrt{\frac{4 \times a^3}{27 \times r^3 \times \kappa}} \quad (1)$$

$$a = \frac{2 \times \sigma}{R_v \times T \times \rho_\omega} \quad (2)$$

Where α (m) is the coefficient of the Kelvin effect, κ is the volume−averaged hygroscopicity, calculated using these values in Table 1, r (m) is the dry diameter, σ is droplet surface tension over water (0.076 N m^{-1}), R_v is the gas constant for water vapor (461.6 J $K^{-1}kg^{-1}$), T (K) is the air temperature, and ρ_ω is the density of water (1000 kg m^{-3}).

Table 2 Hygroscopicity Parameters (κ) in the WRF-Chem Model

Species	Hygroscopicity (κ)
Sulfate	0.5
Ammonium	0.5
Nitrate	0.5
Black carbon	10^{-6}
Primary organic aerosol	0.14

Other inorganics	0.14
Sodium	1.16
Chloride	1.16

The chemical aging process of organic aerosols (OA) is modeled by the volatility basis set (VBS) approach, which was widely used in air quality models to represent complex mixtures of thousands of organic species ~~(Donahue et al., 2006; Shrivastava et al., 2011; Chrit et al., 2018)~~(Donahue et al., 2006; Shrivastava et al., 2011; Chrit et al., 2018). The VBS method classifies compounds according to the effective saturation concentration (~~C~~*c**), which represents the proportion of the ~~componenet~~component in the gas phase to the particle phase ~~(Donahue et al., 2006)~~(Donahue et al., 2006), and species with higher ~~C~~*c** values are more volatile. The oxidation of highly volatile precursors to form relatively low volatile components represents the aging process of OA. OA consists of directly emitted primary organic aerosols and photochemically produced secondary organic aerosols (SOA) ~~(Shrivastava et al., 2011)~~(Shrivastava et al., 2011). In this study, the simplified 2-species VBS mechanism was applied to the simulation of SOA, during which primary organic aerosol was represented by two species based on volatility with effective saturation concentration ~~C~~*c** values (at 298 K and 1 atm) of 10^{-2} and 10^{5} μg m^{-3} ~~(Shrivastava et al., 2011)~~(Shrivastava et al., 2011). Primary organic aerosols with ~~C~~*c** of 10^{5} μg m^{-3} refers to S/IVOC, which is in the gas phase under most atmospheric conditions due to its high volatility, while for those primary organic ~~aerosols~~matters with ~~C~~*c** of 10^{-2} μg m^{-3}, is treated as gas phase as well in the original model. The SOA formed by photochemical oxidation of S/IVOC precursors is called SI-SOA and the SOA formed by oxidation of VOC precursors is named V-SOA. In the simplified 2-species VBS mechanism, SI-SOA (~~C* of 10^{-2} μg m^{-3} is formed by the oxidation reaction of S/IVOC precursors (C* of 10^{5} μg m^{-3}) and OH with an oxidation rate constant of 4×10^{-11} cm^{3} $molec^{-1}$ s^{-1}. A detailed description of 2-species VBS mechanism can be found in Shrivastava et al. (2011).~~*c** of 10^{-2} μg m^{-3}) is formed by the oxidation reaction of S/IVOC precursors (*c** of 10^{5} μg m^{-3}) and OH with

an oxidation rate constant of 4×10^{-11} cm^3 $molec^{-1}$ s^{-1}. The equations for controlling the oxidation of S/IVOC precursors are as follows:

$$POA(g)_{e,c} + OH \rightarrow SI - SOA(g)_{e,c} + 0.15SI - SOA(g)_{e,o} \quad (3)$$

$$POA(g)_{e,o} + OH \rightarrow SI - SOA(g)_{e,o} + OH \quad (4)$$

where POA(g) denotes primary organic aerosols with c^* of 10^5 μg m^{-3}, which reacts with OH to form SI-SOA(g) with c^* of 10^{-2} μg m^{-3}. Subscripts c and o represent the non-oxygen and oxygen parts respectively of given species and e is either the biomass or anthropogenic emission sector. In addition, SVOC and IVOC emissions corresponding to both anthropogenic and biomass burning emissions are derived based on constant emission ratio of S/IVOC to POA (Shrivastava et al., 2011). A detailed description of 2-species VBS mechanism can be found in Shrivastava et al. (2011).

2.3 Model sensitivity formulations

Three sets of sensitivity tests are designed and listed in ~~Table 2~~Table3. The purposes of the three sets of experiments are as follows: (1) Adjust the condensation growth process of ultrafine particles in WRF-Chem model (Base, MAC, POA, NOCD, RACD, with details in Table ~~2~~3).; (2) Explore the effect of SI-SOA yield on CCN (Low-Yield and High-_Yield); (3) Study the effect of nucleation process on CCN under the change of SI-SOA yield (Low-Yield and High-_Yield and their corresponding cases without nucleation parameterization, i.e., Low_nucoff and High_nucoff). Each scenario will be explained in conjunctions with the results.

279 Table ~~2~~ 3 The sensitivity tests involved in this study

Purposes	Simulation scenarios ~~Simulationscenarios~~	Description
Adjust the condensation growth process of ultrafine particles	Base	~~Simulation with the default setting with nucleation coefficient set as 2×10^{-6} s^{-1}, the same as Lai et al. (2022)~~Simulation with the default setting with nucleation coefficient set as 2×10^{-6} s^{-1}, the same as Lai et al. (2022)
	Mass accommodation coefficient (MAC)	It is the same as Base except that the mass adjustment coefficient (α) of gaseous sulfuric acid is adjusted from 0.1 to 0.65.
	POA emission phase (PEP)	It is the same as MAC except that the phase of POA is changed from gas phase to particle phase.
	No condensation (NOCD)	It is the same as PEP except that no NH_4NO_3 condenses on particles below 40 nm.
	Ratio method for condensation (RACD)	~~It is the same as PEP except that the condensation of NH_4NO_3 on particles~~

		~~below 40 nm is reduced according to the ratio of acid particles to total particles reported in Wang et al. (2014).~~It is the same as PEP except that the condensation of NH_4NO_3 on particles below 40 nm is reduced according to the ratio of acid particles to total particles reported in Wang et al. (2014).
Explore the effect of SI-SOA yield on CCN (Explore the effect of nucleation process on CCN under the change of SI-SOA yield)	High-_Yield	Simulation with high oxidation rate of SI-SOA formation with reaction rate constant of 5×10^{-11} cm^3 $molec^{-1}$ s^{-1}
	Low-Yield	Simulation with low oxidation rate of SI-SOA formation with reaction rate constant of 2×10^{-11} cm^3 $molec^{-1}$ s^{-1}
Explore the effect of nucleation process on CCN under the change of SI-SOA yield	High_NUCOFF	Simulations without nucleation parameterizations based on High-_Yield
	Low_ NUCOFF	Simulations without nucleation parameterizations based on Low-Yield

3. Results

3.1 Observational analysis

Based on the criteria ~~(Dal Maso et al., 2005; Kulmala et al., 2012)~~(Dal Maso et al., 2005; Kulmala et al., 2012), NPF is defined as an event with the emergence of a nucleation mode with particle diameters smaller than 25 nm, lasting for 2 hours or more, followed in general by a continuous particle growth. Six NPF events were identified in February 2017 in Qingdao, on the days of 6, 9, 10, 17, 20 and 23 (Fig. 1a), yielding a frequency of ~30% and displaying a typical banana-shaped growth of particles in the particle number size distribution. Compared to a few other studies on NPF frequency in Qingdao, the results in this study are to a large extent consistent with that in the fall of 2012–2013 (30%; ~~(Zhu et al., 2019)~~(Zhu et al., 2019)), slightly higher than that in summer 2016 (22%; ~~(Zhu et al., 2019)~~(Zhu et al., 2019)) and lower than that in spring of 2010 (41%; ~~(Liu et al., 2014c)~~(Liu et al., 2014c). The higher frequency in spring in Qingdao is consistent with the observational results at different stations in the Northern Hemisphere in Nieminen et al. (2018).

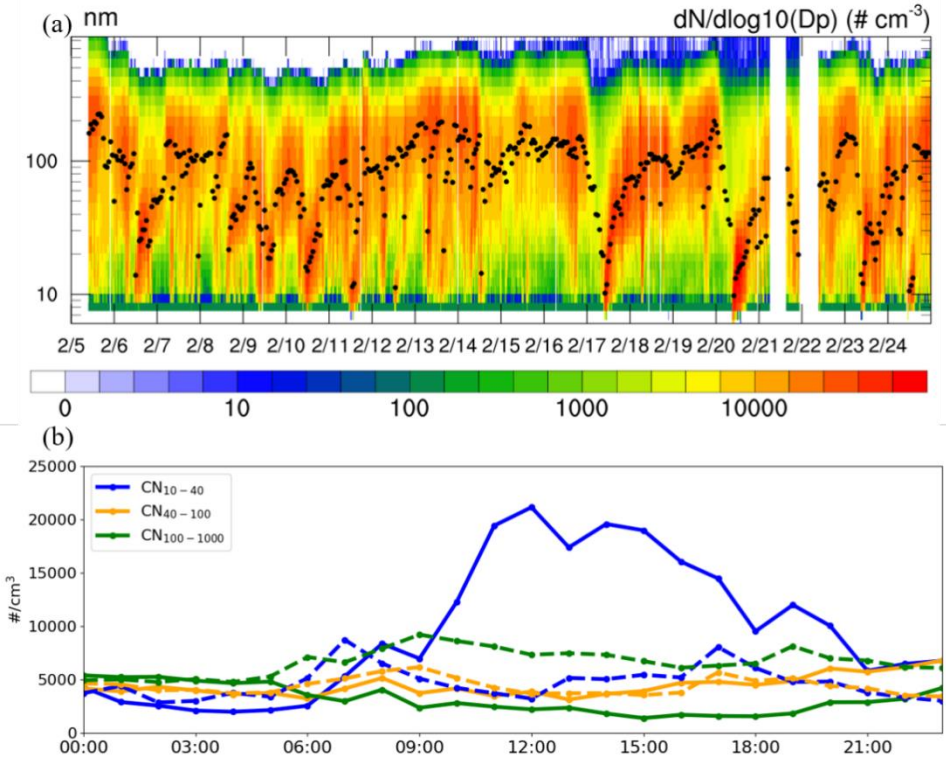

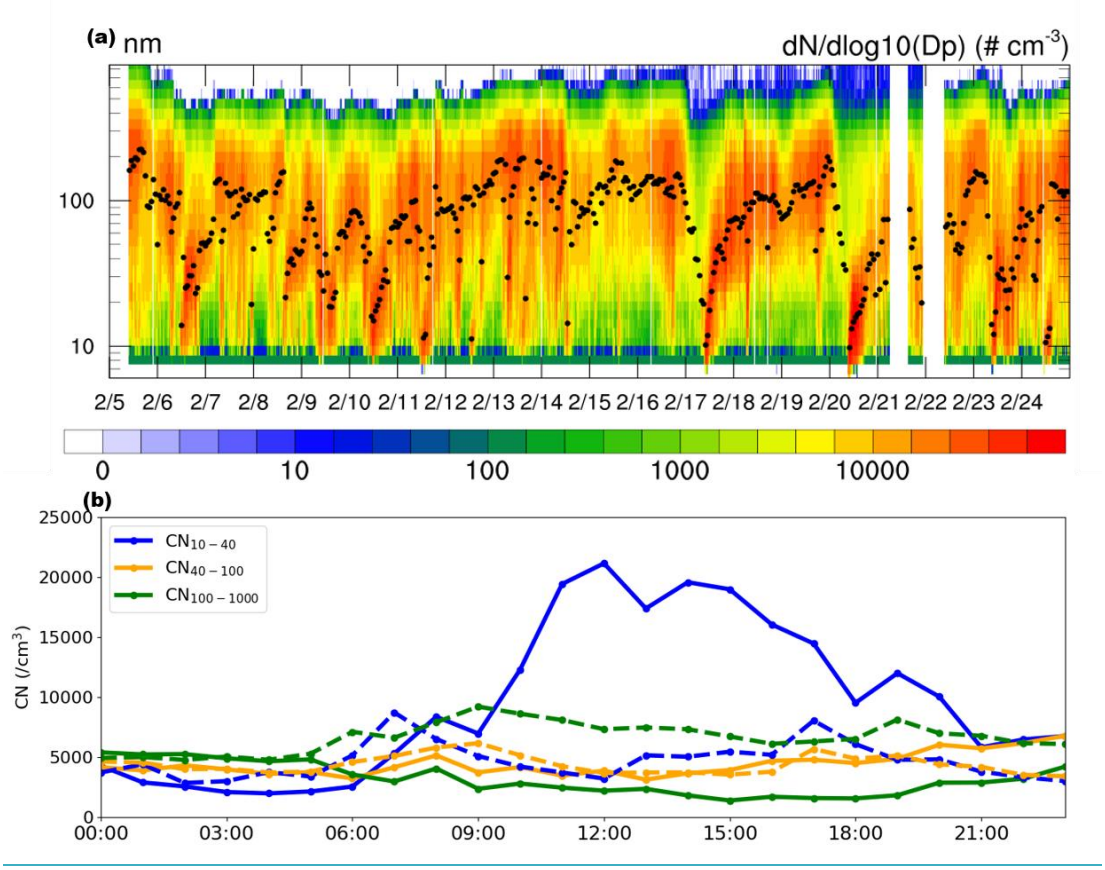

Fig. 1-. Distribution of particle number concentration. (a) Temporal evolution of particle size distributions (colored shading) and geometric median diameter (GMD; dots in black) in Qingdao on February 5-24, 2017. (b) The mean diurnal variation of $CN_{10–40}$ (blue), $CN_{40–100}$ (orange) and $CN_{100–1000}$ (green) composited during the NPF (solid lines) and non-NPF (dashed lines) days on February 5-24, 2017. All times are local times (LT)

During the six NPF events identified in February in Qingdao, the mean diurnal cycle of $CN_{10–40}$ (10–40 nm) particles exhibits triple peaks (solid blue in Fig. 1b), in the morning (8:00 LT), noon (12:00–14:00 LT) and evening (19:00 LT), respectively. A comparable three-peak feature was also observed in earlier years during 2016-2018 in Qingdao ~~(Zhu et al., 2021).~~(Zhu et al., 2021). The morning and evening peaks of $CN_{10–40}$, with values of ~5300 cm^{-3} and ~12000 cm^{-3}, respectively, are likely caused by the primary emissions from traffic and cooking activities ~~(Wu et al., 2021a; Wang et al., 2022; Cai et al., 2020)~~(Wu et al., 2021a; Wang et al., 2022; Cai et al., 2020). The occurrence of NPF starts approximately at 9:00 am LT, accompanied by a substantial increase in $CN_{10–40}$ compared with non-NPF days (solid vs. dashed lines, in blue),

yielding a peak around noon (20000 cm^{-3} during 12:00–14:00 LT). In addition, larger particles (e.g., $CN_{40–100}$ and $CN_{100–1000}$) displayed a slow or no increase in the afternoon.

3.2 Model improvement in particle number concentration simulations

Particle number concentrations, primarily in two ranges of -10–40 nm and 40–100 nm, are commonly simulated with large biases. In the smaller size range (10–40 nm), the particle number concentration is associated with NPF and ~~particles~~particle growth. During NPF, despite differences among the formation mechanisms, H_2SO_4 is considered the common species ~~(Yu, 2005; Lovejoy et al., 2004)~~(Yu, 2005; Lovejoy et al., 2004), which often suffer large biases ~~(Cai et al., 2016; Matsui et al., 2011)~~(Cai et al., 2016; Matsui et al., 2011). In the size range of 40–100 nm, the particle number concentration is primarily affected by the condensation growth of particles below 40 nm, which is closely related to chemical components such as SOA and nitrate. Prior to the evaluation of particle number concentration, we first evaluate the compositions of $PM_{2.5}$ and criteria air pollutants including $PM_{2.5}$, PM_{10}, O_3, SO_2, CO, and NO_2, showing relatively low biases compared to observations (section S1 and Fig. S1 and Fig. S2 of the supporting information).

3.2.1 Bias correction of particle number concentration at 10–40 nm

In this study, as shown in Fig. 2, comparisons of $CN_{10–40}$ between simulations -(red line in Fig. 2a) and observations- (black line in Fig. 2a) results of the six NPF events mentioned in the previous section in Qingdao in February 2017 indicate that -model overestimates $CN_{10–40}$ with mean fractional bias ~~(MFB)~~ of 48%. As one of the major processes affecting the particle number concentration of 10–40 nm, nucleation is governed by the particle nucleation rate of 1 nm particles (cm^{-3} s^{-1}), which is closely associated with the concentration of H_2SO_4. For instance, in a commonly applied activation mechanism, the nucleation rate calculated by $J^* = K_{ACT} \times [H_2SO_4]$~~, where~~. Note that K_{ACT} is the nucleation coefficient considering the physical properties and chemical species of nucleation process under different environments, indicating that a lumped chemical species are included in the scheme reflected primarily in the

nucleation coefficient k, set as 2 × 10^{-6} s^{-1} based on previous studies ~~(Sihto et al., 2006; Riipinen et al., 2007)~~(Sihto et al., 2006; Riipinen et al., 2007)~~. Dong et al. (2019).~~ Dong et al. (2019) simulated NPF occurring in the summer of 2008 in the United States using the ~~NFP~~NPF-explicit WRF-Chem based on the activation mechanism, which overestimated the particle number concentration at 10–63 nm by nearly doubled, even when the K_{ACT} decreased by one order of magnitude (set at a very low value of 10^{-7} s^{-1}). Therefore, it is likely that the overestimation of particle number concentration in the smaller particle size segment is probably due to the bias of simulated sulfuric acid.

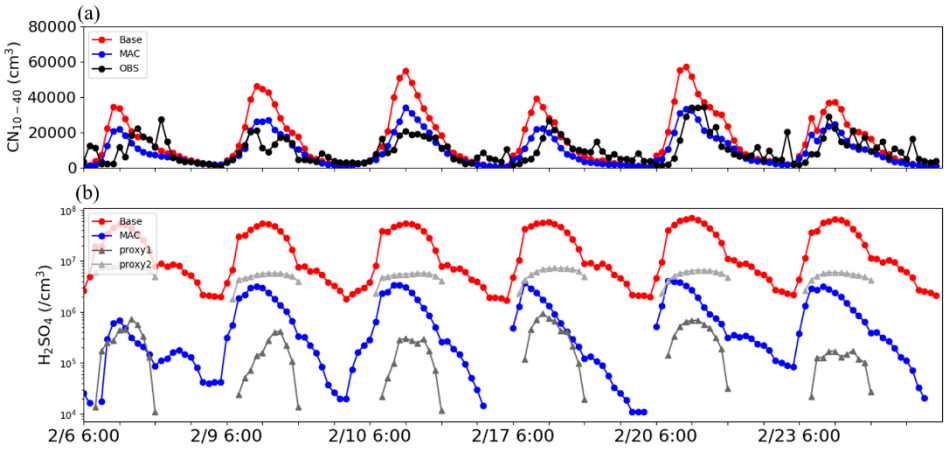

~~Figure~~

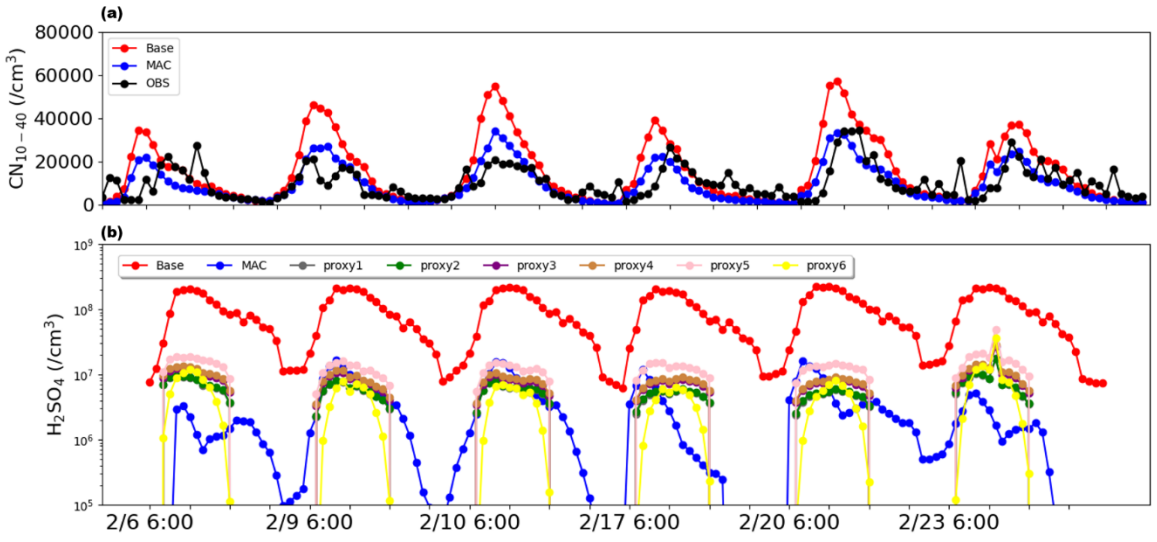

Fig. 2. Time series of (a) $CN_{10–40}$ on NPF days, where red and blue represent Base and MAC simulation results respectively, and black represents observation results, and (b) sulfuric acid gas concentration obtained by simulation and by proxies (dark grey: Eq.

~~1; light grey~~5; green: Eq. ~~2~~6; purple: Eq. 7; brown: Eq. 8; pink: Eq. 9; yellow: Eq. 10). All times are in local times.

Measurement of sulfuric acid gases in the lower troposphere is challenging due to the generally low ambient concentration of sulfuric acid (10^6–10^7 molecule cm^{-3}). Different methods have been proposed to estimate ambient sulfuric acid concentrations based on observations such as SO_2 ~~(Petäjä et al., 2009; Lu et al., 2019)~~(Petäjä et al., 2009; Lu et al., 2019; Mikkonen et al., 2011). ~~For instance, Petäjä et al. (2009) proposed a linear method (Eq. 1) to approximate observed H_2SO_4 concentration in Hyytiala, southern Finland. Moreover, a recent study by Lu et al. (2019) proposed a nonlinear method (Eq. 2), indicating that compared to the linear method in Petäjä et al. (2009), the nonlinear relationship can provide more accurate H_2SO_4 concentration in Beijing during February–March 2018 period.In this study, we adopt both of the above two proxy methods (referred as proxy1 and proxy2~~. For instance, Petäjä et al. (2009) proposed a linear method to approximate observed H_2SO_4 concentration in Hyytiala, southern Finland. Moreover, a recent study by Lu et al. (2019) proposed a nonlinear method to construct a number of proxies for gaseous sulfuric acid concentration (Eq. 5–9), indicating that compared to the linear method in Petäjä et al. (2009), the nonlinear relationship can provide more accurate H_2SO_4 concentration in Beijing during February–March 2018 period. In addition, we also used another sulfuric acid nonlinear proxy (Eq. 10) based on long-term observations in Germany, Finland, the United States, etc. (Mikkonen et al., 2011). In this study, we adopt the above six nonlinear proxy methods (referred as proxy5 to proxy10) to estimate H_2SO_4 in Qingdao.

~~$$[H_2SO_4] = k\frac{[SO_2]\cdot UVB(Glob)}{CS} \quad (1)$$~~

~~$$[H_2SO_4] = 280.05\cdot UVB^{0.14}[SO_2]^{0.4} \quad (2)$$~~

$$[H_2SO_4] = 515.74 \times [SO_2]^{0.38} \times \text{Radiation}^{0.14} \times CS^{0.03} \quad (5)$$

$$[H_2SO_4] = 280.05 \cdot \text{Radiation}^{0.14}[SO_2]^{0.40} \quad (6)$$

$$[H_2SO_4] = 9.95 \times [SO_2]^{0.39} \times \text{Radiation}^{0.13} \times CS^{-0.01} \times [O_3]^{0.14} \quad (7)$$

$$[H_2SO_4] = 14.38 \times [SO_2]^{0.38} \times \text{Radiation}^{0.13} \times [O_3]^{0.14} \quad (8)$$

$$[H_2SO_4] = 0.0013 \times [SO_2]^{0.38} \times \text{Radiation}^{0.13} \times CS^{-0.17} \times ([O_3]^{0.14} + [NO_x]^{0.41}) \quad (9)$$

$$[H_2SO_4] = 8.21 \times 10^{-3} \times [SO_2]^{0.62} \times \text{Radiation} \times (CS \times RH)^{-0.13} \quad (10)$$

where ~~k is an empirically derived factor with value of 2.3×10^{-9} m^2 W^{-1} s^{-1},~~ [SO_2], [O_3] and [NO_x] (molecule cm^{-3}) represents ~~the~~ concentration of observed SO_2, ~~UVB(Glob) and UVB (W m^{-2}) are solar radiation in global~~ O_3 and ~~UV-B range (280-320 nm) radiation~~NO_x, respectively~~.~~. "Radiation" (W m^{-2}) is global radiation. RH (%) is the relative humidity, and CS (s^{-1}) is the condensation sink, which is calculated based on observed particle distribution.

The simulated H_2SO_4 concentration from the Base simulation (dots in Fig. 2b) is compared with observations obtained by proxies (see Fig. 2b), indicating that Base simulations apparently overestimate by one order of magnitude compared to the ~~higher~~ H_2SO_4 estimated by ~~proxy 2~~proxies. The overestimation has been frequently reported previously, i.e., over Beijing ~~(Matsui et al., 2011)~~(Matsui et al., 2011), which ascribes the bias to the overestimation of the SO_2 concentration. In a more recent study, the sensitivity of H_2SO_4 to SO_2 is tested, and the result shows that even when SO_2 is reduced to an unrealistically low level, the simulated H_2SO_4 is still more than one order of magnitude higher than the observed value (Lai et al., 2022), suggesting that the SO_2 concentration cannot fully explain the overestimates.

In addition to the precursor of H_2SO_4, the mass accommodation coefficient (α), representing the probability of impaction of a gaseous molecule on a liquid surface and entering the bulk liquid phase, is another important factor affecting the concentration of sulfuric acid gas. In the public release of WRF-Chem, ~~α~~mass accommodation coefficient is typically set to a low value of 0.1 for all gas species under different volatility during the condensation process, including H_2SO_4 ~~(Davidovits et al., 2004; Zaveri et al., 2008)~~(Davidovits et al., 2004; Zaveri et al., 2008). Recent studies indicate that the low ~~α~~mass accommodation coefficient value may not be applicable to the low volatile gases, which tend to have a mean ~~α~~mass accommodation coefficient value of 0.7 and close to the unity ~~(Krechmer et al., 2017)~~(Krechmer et al., 2017). In fact, an earlier study has indicated based on experimental determination, the mass accommodation coefficient of H_2SO_4 vapor in sulfuric acid aqueous solution was

measured, and the best fit value was 0.65 ~~(Pöschl et al., 1998)~~(Pöschl et al., 1998). Accordingly, a sensitivity simulation was conducted by adjusting the mass accommodation coefficient of H_2SO_4 from 0.1 to 0.65, referred to as MAC.

This simulation brought the H_2SO_4 concentration (see Fig. 2b) much closer to the calculated results from proxies, and the corresponding biases reduced by approximately an order of magnitude. Notably, the MAC simulation decreases the overestimate of sulfuric acid gas concentration, resulting in a lower particle formation rate. The MAC simulation also significantly reduces overestimate of $CN_{10–40}$ (Fig. ~~2b~~2a), and ~~MFB~~mean fractional bias compared to observations decreases from 48% to 1%.

3.2.2 Improvement of particle number concentration simulations at 40–100 nm

The number concentration of particles in the 40–100 nm range is mainly affected by the coagulation and condensation processes. While the coagulation process tends to largely affect ultrafine particles below 10 nm than those with larger sizes ~~(Wu et al., 2011)~~(Wu et al., 2011), the condensation growth of particles during gas-particle partitioning at sizes of 10–40 nm, to a large extent, governs the variations in number concentration of 40–100 nm particles. The condensation process is primarily controlled by gas-particle partitioning of chemical species, which may change the chemical composition of particles, such as organic compounds and inorganics including sulfate, nitrate and ammonium.

Among the species contributing to the condensation growth of particles at 10–40 nm, the organic compounds with ~~with C*~~*c** of 10^{-2} μg m^{-3}~~play~~ play the dominant role ~~(Pierce et al., 2011)~~(Pierce et al., 2011). In the current model setting, ~~there is a total of two volatility sets, including 10^{-2} μg m^{-3} and 10^{5} μg m^{-3}. The~~the low volatile organic matter of 10^{-2} μg m^{-3} comes from two gas-phase sources, including the direct emission of primary organic aerosol (POA) and SOA formed from S/IVOC (SI-SOA), conducive to condensation on particles. While the condensation of gaseous SOA is in general reasonable, the gas phase emissions of POA may be problematic. For instance, previous studies suggested that POA is in gas phase close to the emissions source~~, but~~. However, with rapid dilution and cooling in the atmosphere away from the source, most POA

condenses to particle-phase ~~(Roldin et al., 2011b; Roldin et al., 2011a; Shrivastava et al., 2008)~~(Roldin et al., 2011b; Roldin et al., 2011a; Shrivastava et al., 2008). Therefore, away from the emissions source POA, being in the particle phase, will not be involved in the growth of newly formed particles. Therefore, ~~we assume that low volatility~~ POA ~~is emitted in the~~ may not contribute to particle ~~phase rather than~~growth away from the ~~gas-phase~~emission sources, which caused different size distributions of POA compared to when it was emitted in the gas-phase (Fig. ~~S1a~~S3a vs. Fig. ~~S1b~~S3b). Emitting low volatility POA in the particle phase eliminates the unreasonable quasi-banana shape pattern exhibiting concomitant growth of newly formed particles with increasing mass concentration of POA.

The composition analysis (Fig. ~~S1c~~S3c) in the 10–40 nm particles mass from the model results indicates that organic compounds mentioned above only account for 21% of total mass (sulfates, nitrates, ammonium salts and organics) in this size range and the dominant species is nitrate which accounts for 51% of total mass, exhibiting inconsistencies with the previous studies which in general indicates a much smaller contribution of nitrate. ~~For instance, Liu et al. (2014a)~~For instance, Liu et al. (2014a) suggested that over North China Plain in summer 2009, organic matter accounted for 77% of particles around 30 nm, while the sum of SO_4^{2-}, NO_3^- and NH_4^+ only accounted for 18%. Another study showed that nitrate accounted for 7–8% at urban sites and 17% at rural sites for particles mass in 7–30 nm in the United States in 2007 ~~(Bzdek et al., 2012)~~(Bzdek et al., 2012). Therefore, the potentially too high modeled nitrate fraction in 10–40 nm in this study is tightly associated with the condensation process, with the specific reasons explained below.

The condensation of nitric acid on particles is highly constrained by the particle acidity. The acidity in smaller particles (i.e., 10–40 nm) tends to be higher than that in large particles, primarily due to the larger condensation of H_2SO_4 ~~(Lu et al., 2022)~~(Lu et al., 2022), and particles with sizes greater than 40 nm have a much weaker acidity or are nearly neutral. For example, observed evidence has shown that acidic ultrafine particles account for a large proportion of ultrafine particles from 22 December 2010 to 15 January 2011 in Hong Kong, e.g., 65% for particles within 5.5–30 nm (Wang et

al., 2014).

In the model, a particle is determined to be in solid phase when the ambient relative humidity is lower than the mutual deliquescence relative humidity of the particles ~~(Zaveri et al., 2005; Zaveri et al., 2008)~~(Zaveri et al., 2005; Zaveri et al., 2008), which is in general suitable for particles dominated by inorganics. In the study area, the results indicate that at most conditions relative humidity are relatively low and the particles are in solid phase, in which the condensation process is not affected by particle acidity and the condensation of nitric acid on particles is directly calculated based on the gas-particle equilibrium concentration ~~(Zaveri et al., 2008)~~(Zaveri et al., 2008). However, for particles below 40 nm, the main compositions are likely to be organic matter ~~(Zhu et al., 2014; Ehn et al., 2014)~~(Zhu et al., 2014; Ehn et al., 2014), which tends to be in liquid phase ~~(Virtanen et al., 2011; Cheng et al., 2015)~~(Virtanen et al., 2011; Cheng et al., 2015), under which the condensation of nitric acid is strongly constrained by acidity. Therefore, the phase misrepresentation ignores the weakening effect of acidity on nitric acid condensation, resulting in too high nitrate therein.

To overcome this issue, we propose a ratio method for condensation (RACD) to partition the condensation of nitric acid on particles under 40 nm, by applying a ratio of the number concentration of non-acidic particles to ultrafine particles. The method is based on two assumptions, including: 1) little condensation of nitric acid on particles with strong acidity ~~(Lu et al., 2022)~~(Lu et al., 2022); 2) the condensation of nitric acid on particles is proportional to the ratio of the number concentration of non-acidic ultrafine particles to the total particles, despite the existence of uncertainties. Fig. ~~S2~~S4 depicts the average particle number concentration and acid particle in the 1 to 40 nm range, calculated based on ~~Wang et al. (2014)~~Wang et al. (2014). The ratio of non-acidic particles is 8% for particles below 10 nm, 18% for particles at 10–15.~~8nm~~8 nm, 30% for particles at 15.8–25.1nm, and 55% for particles at 25.1–39.~~8nm~~8 nm (Fig. ~~S2~~S4). Note that the ratio is based on measurements acquired at a single site in Hong Kong, therefore more observational studies are needed to warrant the robustness of the method. Alternatively, the condensation of nitric acid on particles in bins from 1nm to 40 nm is completely suppressed, referred to as NOCD.

The simulation results based on the two methods (RACD and NOCD) are ~~-~~shown in Fig. 3. Compared to MAC, RACD simulations reduce previously noted overestimation of ~~PNC~~particle number concentration in the 40–100 nm size range (Fig. 3b), with the ~~MFB~~mean fractional bias decreases from 83% to 63%. In addition to the amount of nitrate condensation during particle growth mentioned above, the overestimation of particle number concentrations in the 40–100 nm range may be attributed to nucleation process. More specifically, in the H_2SO_4-H_2O binary nucleation mechanism used in this study, when the concentration of sulfuric acid gas is reduced (Section 3.2.1), the resulting decrease in nucleation rate leads to a slight decrease in particle number concentration at 40–100 nm relative to Base (~~MFB~~mean fractional bias from 98% to 83%). Apart from that, it may also be related to the choice of nucleation parameterization scheme. For example, using a global chemical transport model GEOS-Chem~~, Yu et al. (2015)~~ with a nucleation mechanism in which formation rate is a function of the concentrations of sulfuric acid and low-volatility organics, Yu et al. (2015) overestimated the concentration of particles in the 10–100 nm range by 161% at nine sites in the summer in North America. A possible explanation for this overestimation was given by the uncertainty of the predicted concentration of organic compounds involved in organics-mediated nucleation parameterization. After they switched to another scheme of the ion-mediated nucleation mechanism without organic matter, the number becomes 27% lower than the observations ~~(Yu et al., 2015)~~(Yu et al., 2015). The test based on different schemes is beyond the scope of the study, which is therefore not investigated.

Moreover, the overestimation of particles over 100 nm ($CN_{100–1000}$; Fig. 3c), which have a strong influence on CCN, also decrease in the RACD simulation. Thus, the ~~MFB~~mean fractional bias decreases from 25% (MAC) to 1%. Note that the slight increase of $CN_{10–40}$ through the application of RACD, can be linked to the decrease of nitrate condensation, and leads to weakened particle growth and enhanced particle number concentration at 10–40 nm (Fig. 3a). The alternative method by completely removing the nitrate condensation (NOCD) yields even better performance in particle number concentration of 40–100 nm (~~MFB~~mean fractional bias of 34%), indicating the

feasibility by reducing the nitrate condensation. The proportion of nitrate simulated by RACD is 23%, closer to values reported in past observations ~~(Bzdek et al., 2011; Bzdek et al., 2012)~~(Bzdek et al., 2011; Bzdek et al., 2012), while the nitrate (1%) in the scenario of NOCD seems to be too low. Considering the limited observational information obtained based on previous studies, RACD is applied in this study.

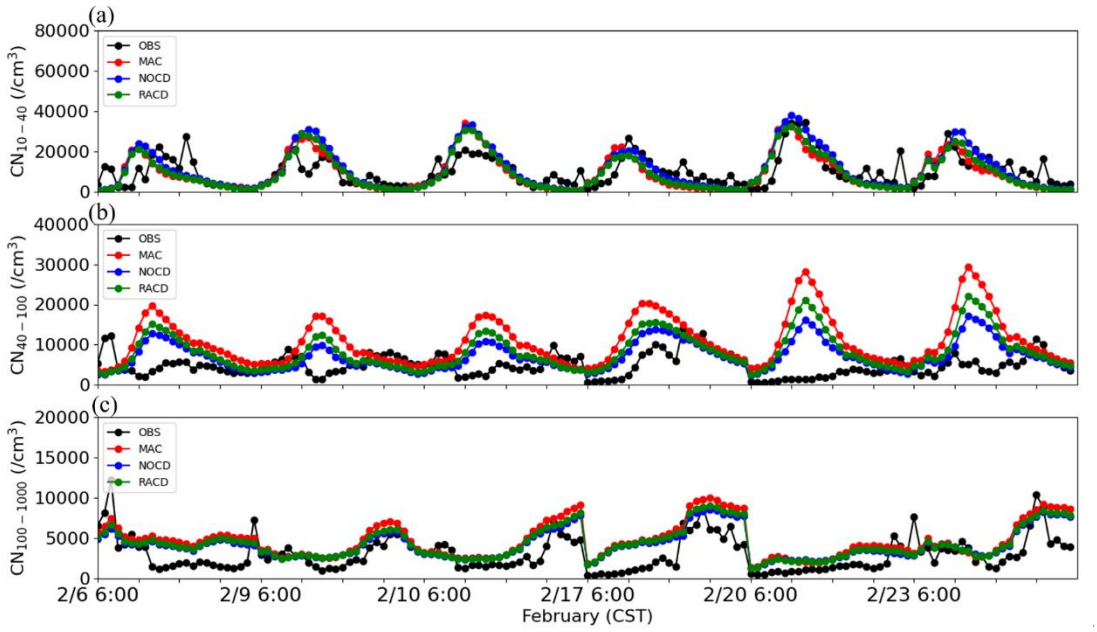

~~Figure 3~~In addition to Qingdao, we evaluate the model performance over a few other sites, including one site over urban Beijing and the other one over the rural area of Gucheng, yielding consistent improvements in model simulations (Section S2; Fig. S6-S8). Moreover, we select another empirical scheme, e.g., kinetics, and one classical nucleation scheme, indicating the empirical scheme of activation scheme is in general a good option in this study (Section S2; Fig. S9-S11; Table S1-3).

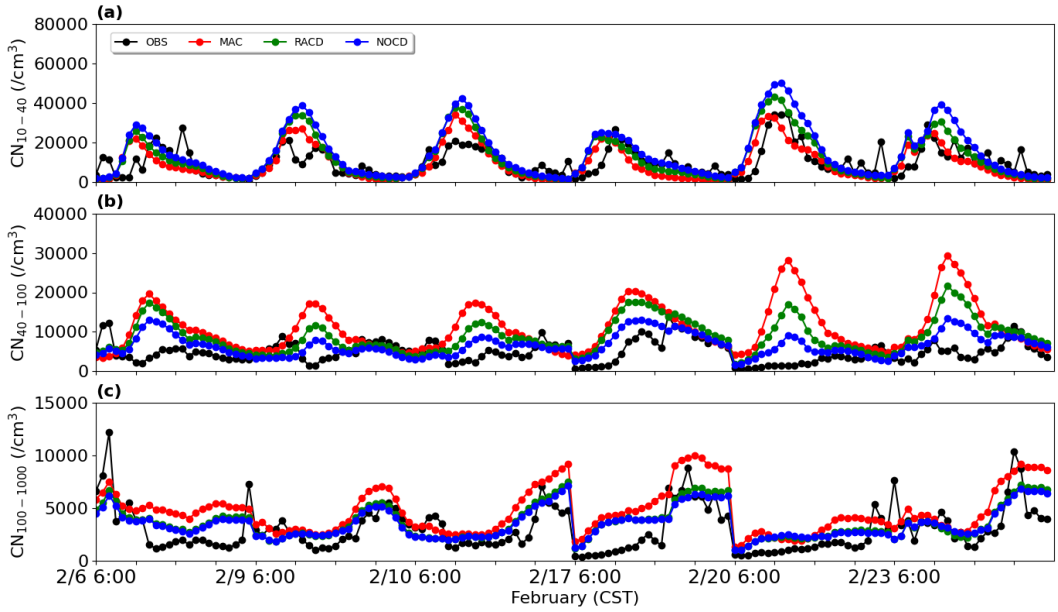

Fig. 3. The time series of (a) $CN_{10–40}$, (b) $CN_{40–100}$ and (c) $CN_{100–1000}$ on NPF days in Qingdao on February 5-24 simulated from MAC (marked in red), NOCD (marked in blue) and RACD (marked in green) as well as from observations (OBS) (marked in black). All times are local time.

3.3 Substantial contributions of SI-SOA to CCN

Compared with the original model setting, after adjusting the growth process of ultrafine particles (RACD), the number concentration of particles tend to decrease, especially for particles above 40 nm. Ultrafine particles above 40 nm are important sources of CCN ~~(Dusek et al., 2006)~~(Dusek et al., 2006), in this way, the number concentration of CCN also tends to decline. In addition, in the Base case, we found that the model overestimated $CCN_{0.4\%}$ and $CCN_{0.6\%}$, with ~~MFB~~mean fractional bias being 64% and 87%, respectively. After adjusting the condensation growth process of ultrafine particles, under high supersaturation (i.e., $CCN_{0.4\%}$ and $CCN_{0.6\%}$), the capability of the model in reproducing the CCN is improved. RACD reduces the overestimation of $CCN_{0.4\%}$ and $CCN_{0.6\%}$, with ~~MFB~~mean fractional bias reduced to 30% and 56%, respectively, although the overestimates still exist (Figs. ~~S3b~~S5b, c). However, for low supersaturation (i.e., $CCN_{0.2\%}$), the decrease of number concentration of CCN

is too large, and ~~MFB~~mean fractional bias decreases from 7% to -45% (~~Figs. S3a~~Fig. S5a), therefore the bias will be further adjusted later.

In addition to the growth process, the remaining overestimate of CCN under high SS and underestimate of CCN over low SS is likely to be influenced by the chemical compositions involved in the activation of ultrafine particles into CCN. Specifically, ultrafine particles can grow up to CCN size under certain SS (Pierce and Adams, 2007). This process is influenced by both particle size and hygroscopicity, and hygroscopicity is closely related to the chemical composition of particles (Petters and Kreidenweis, 2007). In particular, inorganic compounds generally increase particle hygroscopicity, increasing CCN. SOA has dual effects on CCN since it decreases particle hygroscopicity but also promotes growth of particles, and these two effects are competitive with each other (Wu et al., 2015; Zaveri et al., 2021). Ultrafine particles must grow to a critical size to be activated into CCN ~~(Dusek et al., 2006)~~(Dusek et al., 2006). SOA act as a major contributor in promoting the condensational growth of ultrafine particles to the critical size, facilitating particles activation into CCN. In contrast, SOA tends to reduce the hygroscopicity of particles, leading to a diminished ability of activation to CCN (Wu et al., 2015). These two competing effects work together and modulate the number of CCN. Moreover, considering that SI-SOA is the main SOA component on ultrafine particles (Fig. ~~S3d~~S5d), the effect of SI-SOA on CCN is therefore explored in this study.

Considering SI-SOA is a product of S/IVOC oxidation, the oxidation rate of S/IVOC is tightly associated with CCN, which likely affects the bias of CCN. In the original model setup, the oxidation rate is set to be a constant of 4×10^{-11} cm^3 $molec^{-1}$ s^{-1} for all S/IVOC. However, a recent study ~~(Wu et al., 2021b)~~(Wu et al., 2021b) proposed that the oxidation rate can be as high as ~~-~~ 5×10^{-11} cm^3 $molec^{-1}$ s^{-1} such as for polycyclic aromatic hydrocarbons (PAHs), close to the original model value, but can be as low as half (i.e., 2×10^{-11} cm^3 $molec^{-1}$ s^{-1}) of the original modeling setting for S/IVOC species except PAHs (O-S/IVOCs). It is noteworthy that the oxidation rates of 5×10^{-11} and 2×10^{-11} in general represent the upper and lower bounds ~~(Zhao et al., 2016; Wu et al., 2021b)~~(Zhao et al., 2016; Wu et al., 2021b).

To delve into how oxidation rates affect CCN, we set up a few numerical experiments (Table 2) to investigate the response of CCN to the oxidation rate of S/IVOC at three supersaturations (0.6%, 0.4%, 0.2%), including cases of High_Yield and Low_Yield. As it is shown in Fig. 4, decreasing the oxidation rate (Low_Yield) leads to a reduction of ~10% of CCN at high supersaturation (i.e., CCN0.6%) as compared to the High_Yield simulation. This behaviour is a consequence of the decrease of particle number concentrations associated with Low_Yield, particular of the particles close to the critical ~~dameter~~diameter (40–100 nm). In this case, the effect of particle size dominates the hygroscopicity. In contrast, at a lower supersaturation ($CCN_{0.2\%}$), CCN increases by 42% when the oxidation rate is switched from a high to a low value, which is due to the smaller fraction of SI-SOA contributing to particulate mass when the ~~oxidate~~oxidation rate is low. In this case, relative to SOA, a larger fraction of other particle constituents such as inorganics, increase the volume weighted particle hygroscopicity ~~(Dusek et al., 2006)~~(Dusek et al., 2006) which causes the increase of CCN number. This means that the effect of hygroscopicity on CCN surpasses the influence on particle size at low supersaturations. This conclusion is consistent with the observation conducted by ~~Ma et al. (2016)~~Ma et al. (2016) in the North China Plain in 2013, which suggested that along with the decrease of SS, the particles that can be activated to CCN is more sensitive to changes of particle hygroscopicity.

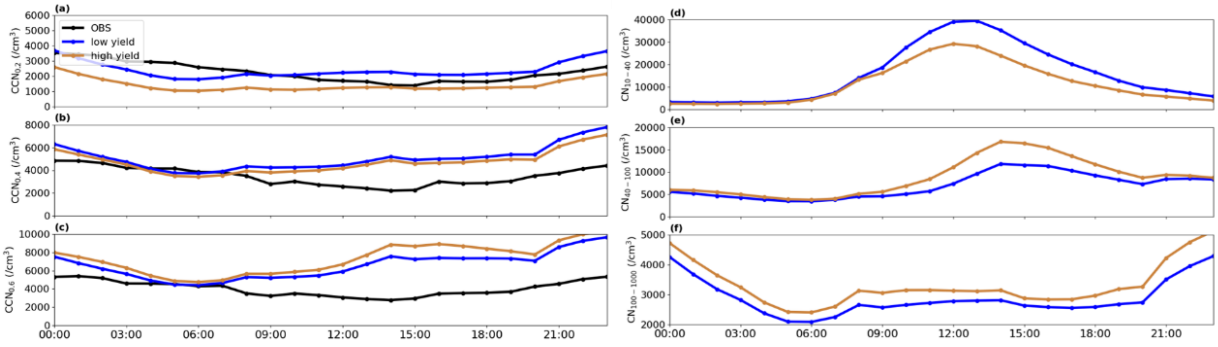

~~Figure~~

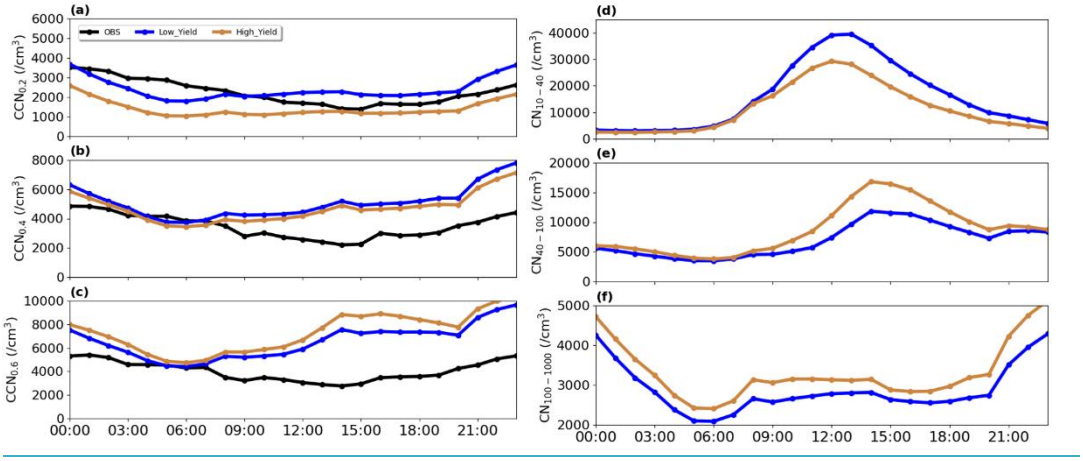

Fig. 4. Average diurnal variation of (a) $CCN_{0.2\%}$, (b) $CCN_{0.4\%}$ and (c) $CCN_{0.6\%}$ and (d) $CN_{10–40}$, (e) $CN_{40–100}$, (f) $CN_{100–1000}$ on NPF days in Qingdao on February 5-24, 2017, in Low-yield and High-yield simulations, shown as blue and brown lines, and black lines represent observation results.

Furthermore, compared to the high yield of SI-SOA, the low SI-SOA yield results in a high CCN concentration under low SS and low CCN concentration under high SS. Therefore, both the underestimates of $CCN_{0.2\%}$ (~~MFB~~mean fractional bias of -45%) and overestimates of $CCN_{0.6\%}$ (~~MFB~~mean fractional bias of 56%) mentioned above are improved, with ~~MFB~~mean fractional bias of $CCN_{0.2\%}$ and $CCN_{0.6\%}$ reaching 7% and 43%, respectively (~~Figs~~Fig. 4a,c). This result suggests that the oxidation rate of S/IVOC is possibly closer to the low value, which is ~~understandble based on Wu et al. (2021b)~~understandable based on Wu et al. (2021b), who found that the amount of O-S/IVOCs, which corresponds to a low oxidation rate, is in general much larger (i.e., 20 times) than that of PAHs with a high oxidation rate.

In addition to the single site of Qingdao, we further explore the impact of SI-SOA yield on CCN from a larger spatial coverage (Fig. 5). Consistent with the mechanism revealed over Qingdao, even from a larger spatial perspective, a lower oxidation rate of S/IVOC essentially enhances CCN at a lower SS (e.g., $CCN_{0.2\%}$; Fig. 5a) with the highest increase over ~~north~~North China Plain area (~~Figs~~Fig. 5a), and weakens CCN (i.e., by 10–20% over Beijing-Tianjin-Hebei) at a higher SS (~~Figs~~Fig. 5c), particularly over the dense emission area (Fig. ~~S4~~S12). It is worth noting that in the 2-species VBS

mechanism used in our study, all S/IVOC in the inventory is calculated based on a constant emission ratio of S/IVOC to POA from all source categories ~~(Shrivastava et al., 2011)~~(Shrivastava et al., 2011), which may miss part of S/IVOC due to different emission ratios of POA from different source ~~(Chang et al., 2022)~~(Chang et al., 2022)~~.~~. In addition, the simplified VBS mechanism used in our study does not take into account the multi-step oxidation of organic species, which may introduce some uncertainties. To be more specific, in the 2-species VBS mechanism, SI-SOA with effective saturation concentrations (c^*) of 10^{-2} μg m^{-3} is formed by the vapor phase oxidation of S/IVOC vapors with c^* of 10^{5} μg m^{-3}, reducing volatility by 7 orders of magnitude. The process of one-step oxidation does not mean to represent a physical process, but to parameterize the mean effect of a complex process of SOA formation (Shrivastava et al., 2011). However, in the real atmosphere, the gaseous VOCs often undergo multi-generational oxidation to form SOA (Garmash et al., 2020), during which the properties and composition of SOA change substantially.

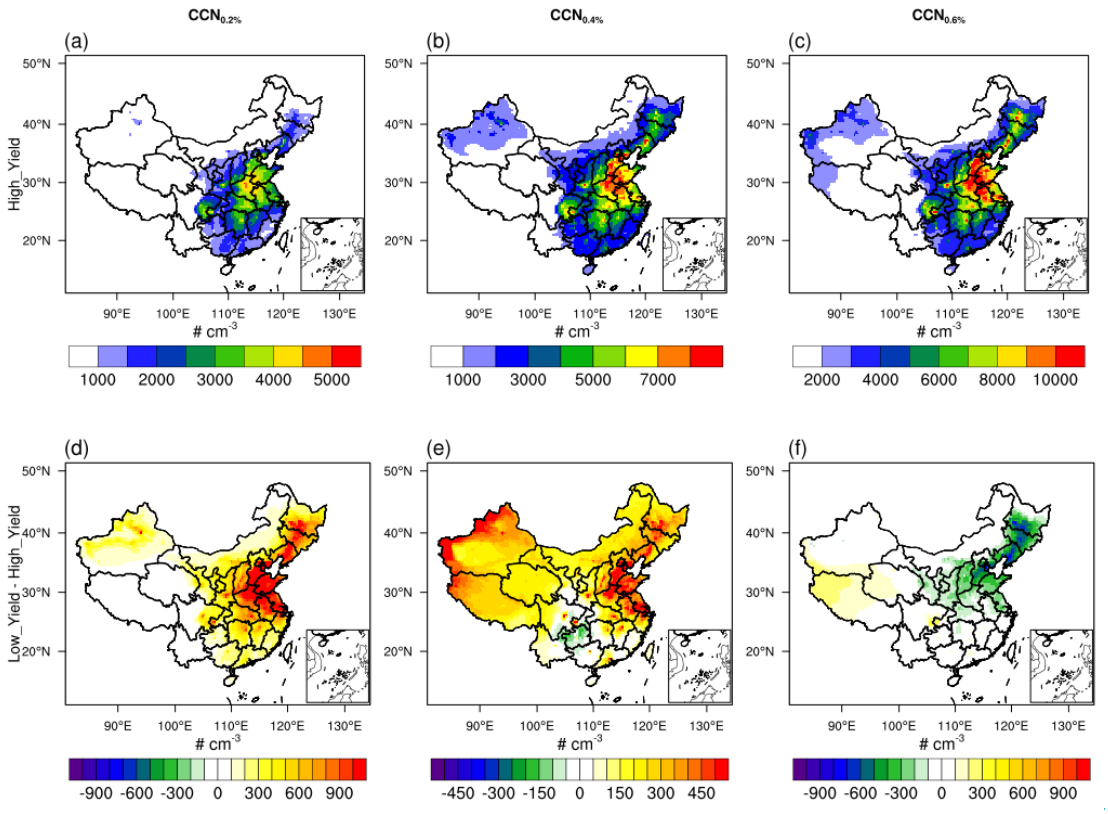

657

658 Figure

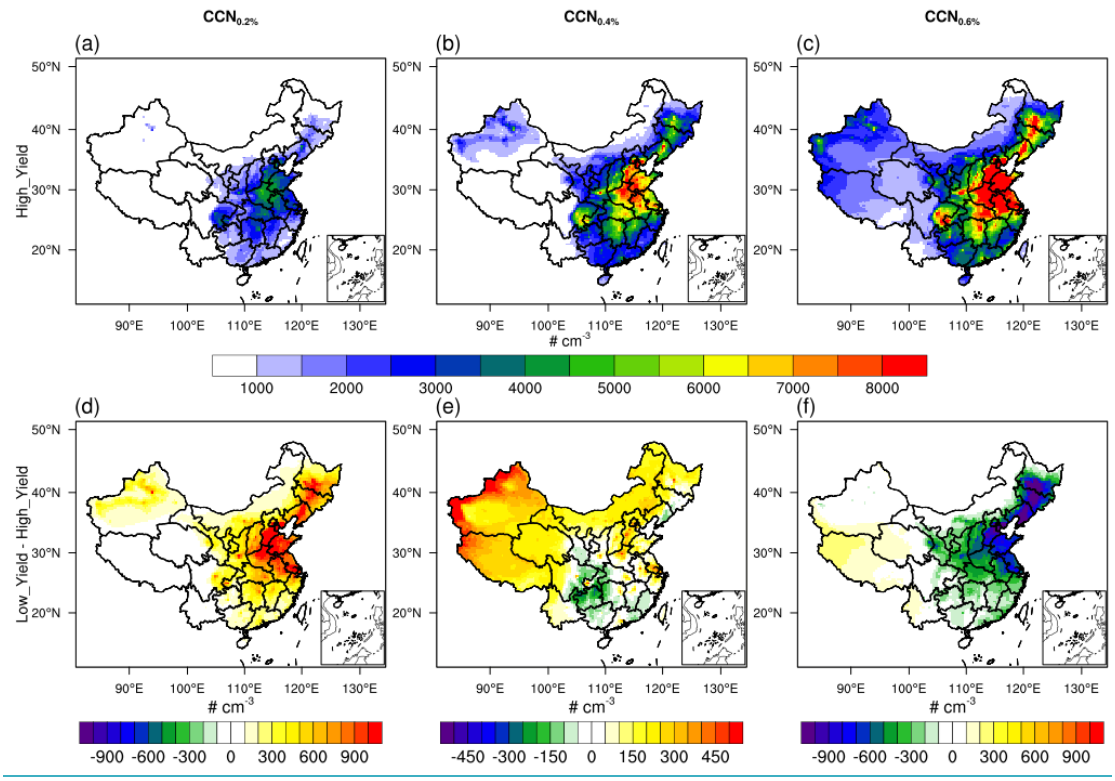

659

660 Fig. 5. Spatial distributions of CCN concentrations at different supersaturations (SS),

661 (a) and (d) are $CCN_{0.2\%}$, (b) and (e) are $CCN_{0.4\%}$, and (c) and (f) are $CCN_{0.6\%}$. The top

panels exhibit the results from the High_Yield simulation, and the bottom panels shows the difference between the Low_Yield and High_Yield simulations.

3.4 Contribution of nucleation to CCN under different SI-SOA yields

Considering the importance of nucleated particles on CCN ~~(Yu et al., 2020; Westervelt et al., 2013)~~(Yu et al., 2020; Westervelt et al., 2013), we further investigate the influence of nucleation on CCN under different SI-SOA yield conditions discussed above.

As shown in Fig. 6, in simulations close to the original model setting (High_Yield), when SS is low (i.e., SS=0.2%), the nucleation process tends to reduce the CCN by ~10–50%. In contrast, when the SS is high (0.6%), the nucleation results in a significant increase in CCN in most regions of China. When the yield of SI-SOA is adjusted to a lower level, the nucleation process has a positive contribution to CCN under both low and high SS. Especially, when SS is low (0.2%), the sign reversal, i.e., from negative (Fig. 6a) to positive (Fig. 6d) ~~contribution~~contributions of NPF to CCN along with the decrease of SI-SOA yield, i.e., ~~-~~the increase is concentrated in the eastern China with an average of 10–20%.~~-~~ The primary mechanism lies in that along with the decrease of SI-SOA yield, the smaller fraction of SI-SOA yields an increase in hygroscopicity, which surpasses the suppression effect on particle growth due to reduced SI-SOA formation. In the real atmosphere, when the supersaturation is usually low, e.g. about ~0.1% in polluted areas ~~(Kalkavouras et al., 2019; Hudson and Noble, 2014)~~(Kalkavouras et al., 2019; Hudson and Noble, 2014), CCN will likely reduce with increasing oxidation rate of S/IVOC and corresponding SI-SOA formation.

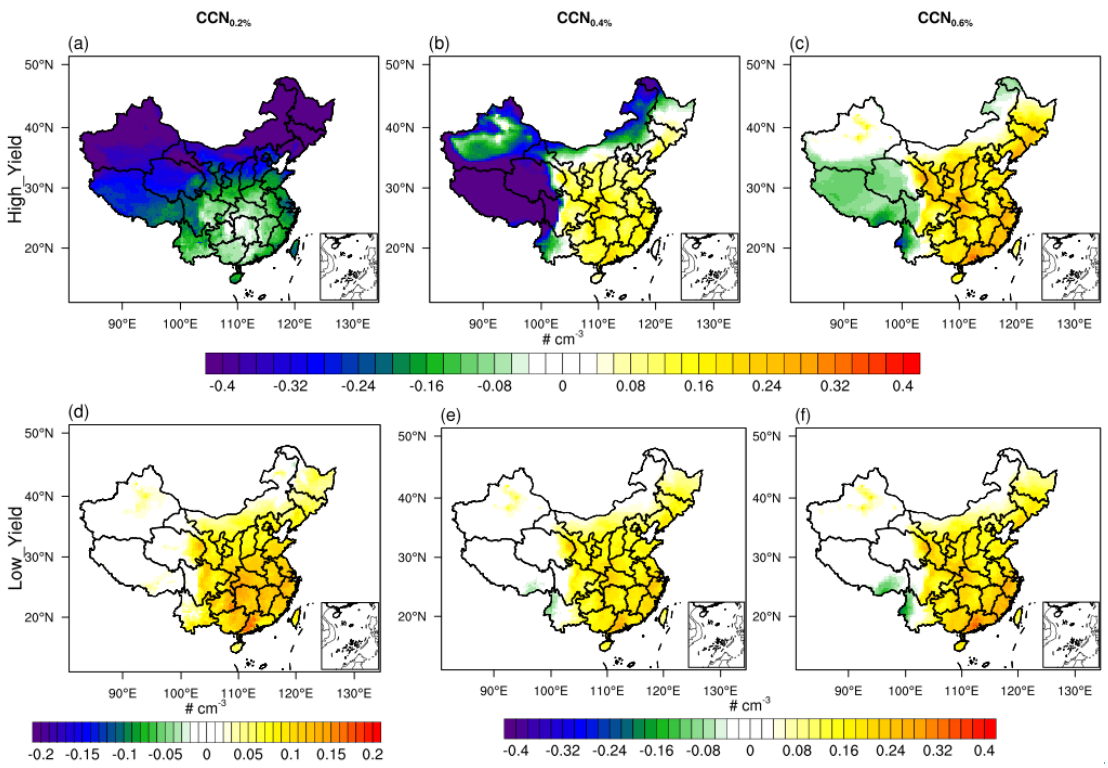

685

686 ~~Figure~~

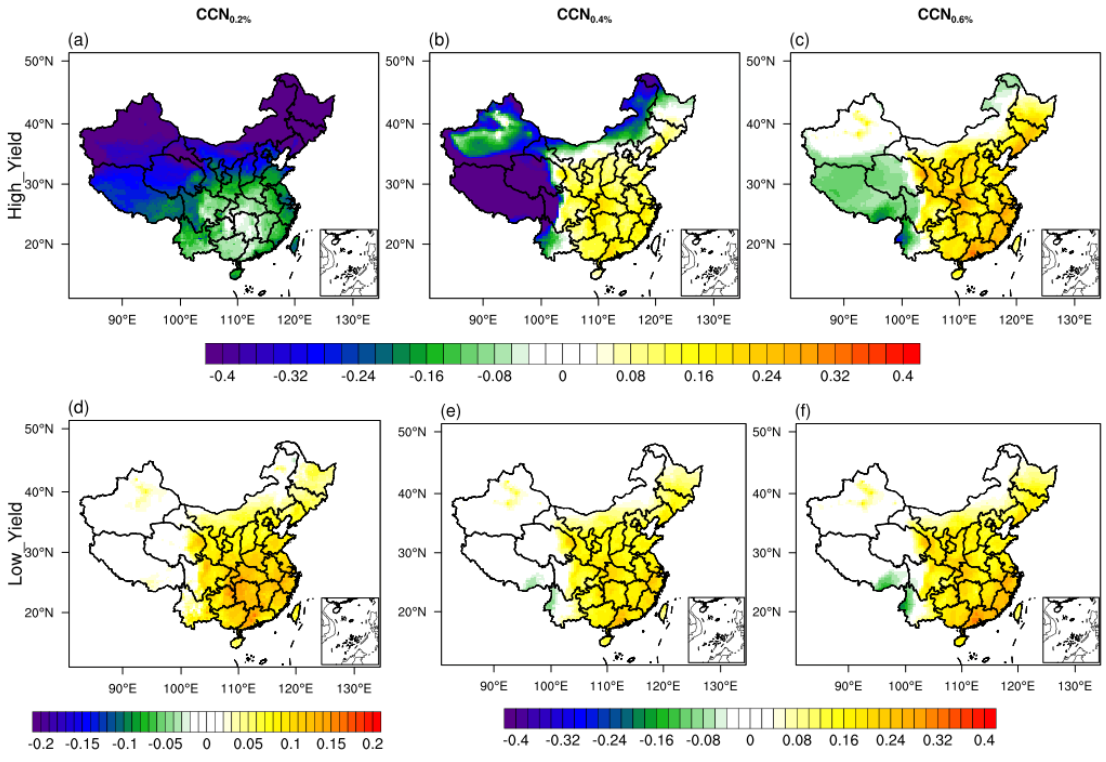

687

688 Fig. 6. Spatial distribution of contribution of nucleation to CCN calculated by the ratio

689 of the difference between the parameterization with and without nucleation to the

690 parameterization with nucleation under different SI-SOA yields in China in February

2017. (a), (d) is $CCN_{0.2\%}$,(b), (e) is $CCN_{0.4\%}$,(c), (f) is $CCN_{0.6\%}$.The upper panel and lower panel represent High_Yield and Low_Yield simulation respectively.

In addition to the linear-H_2SO_4 nucleation mechanism, one more empirical scheme of kinetics nucleation is selected, which assumes that the nucleation rate is proportional to the square of the concentration of sulfuric acid ($J = K[H_2SO_4]^2$), to investigate the effect of nucleation on CCN. Substantially positive contributions of nucleation to CCN is found when the low SI-SOA yield is applied, consistent with what was shown based on the linear-H_2SO_4 nucleation scheme (Fig. S13). However, nucleation contributes positively to CCN even when the SI-SOA yield is high in the quadratic-H_2SO_4 nucleation scheme (e.g., kinetics nucleation scheme). When more sulfuric acid molecules participate in nucleation under this scheme than the linear-H_2SO_4 nucleation scheme, the particles are more easily hygroscopically activated to CCN, which is equivalent to the effect of a reduction in organic components in the linear-H_2SO_4 nucleation scheme (e.g., activation-type nucleation scheme). The results from this study show the importance of assessing the simulated effects of the nucleation scheme on not only the formation and growth process of particles but also climate factors such as CCN using observations.

Conclusions

In this study, WRF-Chem explicit-NPF ~~simiulations~~simulations are used to investigate the observed wintertime NPF events and their contribution to CCN in China. Based on observations in a typical coastal city of Qingdao, we identify high biases of the model simulated CN and CCN concentrations. Therefore, we updated and improved the parameterization setting on particle growth in the model, mainly including: (1) adjusting the mass accommodation coefficient (α) to from the default value of 0.1 to 0.65, an important parameter for sulfuric acid condensation; (2) proportionally reducing the condensation amount of nitric acid on particles below 40 nm, (3) changing the emitted low-volatility POA from gas to particle. Through these adjustments, the

capability of the model in reproducing CN and CCN is substantially improved, leading to better agreement with the observed results, which significantly reduces the overestimation of $CN_{10–40}$ (~~MFB~~mean fractional bias decreases from 48% to 1%) and $CN_{40–100}$ (~~MFB~~mean fractional bias decreases from 98% to 63%).

For CCN, due to the crucial role of SI-SOA in promoting the growth of ultrafine particles, on the basis of previous studies, we lower the oxidation rate of S/IVOC and hence the production rate of SI-SOA, which weakens the growth of particles to reach the critical size of CCN activation, but enhances particulate hygroscopicity favoring the activation to CCN. When the yield of SI-SOA is adjusted to the lower bound of literature value, $CCN_{0.6\%}$ is reduced by ~10% and is closer to observations. At low SS ($CCN_{0.2\%}$), the decrease of SI-SOA yield has greater effects on the increase of particle hygroscopicity compared to the effect of the reduction of particle size due to the decrease of condensation growth. It results in an increase of CCN (as large as ~42%) in better agreement with observations. Under low SS conditions, common in the atmosphere, a 2.5-fold reduction in SI-SOA yield results in a substantial increase of CCN that switches from a negative ~~contributon~~contribution of new particle formation to CCN from -50%~-10% to a positive contribution of 10~20%. The substantial contribution of new particle formation to CCN under low SS and SI-SOA is applicable to other mechanisms such as kinetics.

Competing interests. At least one of the (co-)authors is a member of the editorial board of Atmospheric Chemistry and Physics.

Acknowledgements. This research was supported by grants from the National Natural Science Foundation of China (42122039) and Fundamental Research Funds for the Central Universities (202072001). Y.W. was supported by the National Science Foundation Atmospheric Chemistry Program. M.S. was supported by the U.S. Department of Energy (DOE) Office of Science, Office of Biological and

Environmental Research (BER) through the Early Career Research Program and the Atmospheric System Research (ASR) program.

References:

Arghavani S, Rose C, Banson S, et al. 2022. The Effect of Using a New Parameterization of Nucleation in the WRF-Chem Model on New Particle Formation in a Passive Volcanic Plume. Atmosphere [J], 13(1): 15.

Bergman T, Laaksonen A, Korhonen H, et al. 2015. Geographical and diurnal features of amine-enhanced boundary layer nucleation. Journal of Geophysical Research: Atmospheres [J], 120(18): 9606-9624.

Buchholz R R, Emmons L K, Tilmes.S 2019. The CESM2 Development Team., 2019. CESM2.1/CAM-Chem Instantaneous Output for Boundary Conditions. UCAR/NCAR - Atmospheric Chemistry Observations and Modeling Laboratory.

Bzdek B, Zordan C, Luther G, et al. 2011. Nanoparticle Chemical Composition During New Particle Formation. Aerosol Science and Technology [J], 45(1041-1048.

Bzdek B R, Zordan C A, Pennington M R, et al. 2012. Quantitative Assessment of the Sulfuric Acid Contribution to New Particle Growth. Environmental Science & Technology [J], 46(8): 4365-4373.

Cai C, Zhang X, Wang K, et al. 2016. Incorporation of new particle formation and early growth treatments into WRF/Chem: Model improvement, evaluation, and impacts of anthropogenic aerosols over East Asia. Atmospheric Environment [J], 124(262-284.

Cai J, Chu B, Yao L, et al. 2020. Size-segregated particle number and mass concentrations from different emission sources in urban Beijing. Atmos. Chem. Phys. [J], 20(21): 12721-12740.

Carter W 2000. Documentation of the SAPRC-99 Chemical Mechanism for VOC Reactivity Assessment. Final Report to California Air Resources Board [J].

Chang X, Zhao B, Zheng H, et al. 2022. Full-volatility emission framework corrects missing and underestimated secondary organic aerosol sources. One Earth [J], 5(403-412.

Chang Y, Gao Y, Lu Y, et al. 2021. Discovery of a Potent Source of Gaseous Amines in Urban China. Environmental Science & Technology Letters [J], 8(9): 725-731.

Chen F, Dudhia J 2000. Coupling an Advanced Land-Surface/Hydrology Model with the Penn State/NCAR MM5 Modeling System. 129(

Cheng Y, Su H, Koop T, et al. 2015. Size dependence of phase transitions in aerosol nanoparticles. Nature Communications [J], 6(1): 5923.

Chrit M, Sartelet K, Sciare J, et al. 2018. Modeling organic aerosol concentrations and properties during winter 2014 in the northwestern Mediterranean region. Atmos. Chem. Phys. [J], 18(24): 18079-18100.

Chu B, Kerminen V-M, Bianchi F, et al. 2019. Atmospheric new particle formation in China. Atmospheric Chemistry and Physics [J], 19(115-138.

Dal Maso M, Kulmala M, Riipinen I, et al. 2005. Formation and growth of fresh atmospheric aerosols: Eight years of aerosol size distribution data from SMEAR II, Hyytiälä, Finland. Boreal Environment Research [J], 10(323-336.

792 Davidovits P, Worsnop D R, Jayne J T, et al. 2004. Mass accommodation coefficient of water vapor on
793 liquid water. Geophysical Research Letters [J], 31(22).
794 Donahue N M, Robinson A L, Stanier C O, et al. 2006. Coupled Partitioning, Dilution, and Chemical
795 Aging of Semivolatile Organics. Environmental Science & Technology [J], 40(8): 2635-2643.
796 Dong C, Matsui H, Spak S, et al. 2019. Impacts of New Particle Formation on Short-term Meteorology
797 and Air Quality as Determined by the NPF-explicit WRF-Chem in the Midwestern United States.
798 Aerosol and Air Quality Research [J], 19(2): 204-220.
799 Dusek U, Frank G P, Hildebrandt L, et al. 2006. Size Matters More Than Chemistry for Cloud-Nucleating
800 Ability of Aerosol Particles. Science [J], 312(5778): 1375-1378.
801 Ehn M, Thornton J, Kleist E, et al. 2014. A large source of low-volatility secondary organic aerosol.
802 Nature [J], 506(476-479.
803 Fanourgakis G S, Kanakidou M, Nenes A, et al. 2019. Evaluation of global simulations of aerosol particle
804 and cloud condensation nuclei number, with implications for cloud droplet formation. Atmos.
805 Chem. Phys. [J], 19(13): 8591-8617.
806 Gordon H, Kirkby J, Baltensperger U, et al. 2017. Causes and importance of new particle formation in
807 the present-day and preindustrial atmospheres. 122(16): 8739-8760.
808 Grell G A 1993. Prognostic Evaluation of Assumptions Used by Cumulus Parameterizations. Monthly
809 Weather Review [J], 121(3): 764-787.
810 Guo S, Hu M, Zamora M L, et al. 2014. Elucidating severe urban haze formation in China. Proceedings
811 of the National Academy of Sciences [J], 111(49): 17373-17378.
812 Hong S-Y, Noh Y, Dudhia J 2006. A New Vertical Diffusion Package with an Explicit Treatment of
813 Entrainment Processes. Monthly Weather Review - MON WEATHER REV [J], 134(
814 Hudson J G, Noble S 2014. CCN and Vertical Velocity Influences on Droplet Concentrations and
815 Supersaturations in Clean and Polluted Stratus Clouds. Journal of the Atmospheric Sciences [J],
816 71(1): 312-331.
817 Iacono M, Delamere J, Mlawer E, et al. 2008. Radiative Forcing by Long-Lived Greenhouse Gases:
818 Calculations with the AER Radiative Transfer Models. Journal of Geophysical Research [J],
819 113(
820 Jimenez J L, Canagaratna M R, Donahue N M, et al. 2009. Evolution of Organic Aerosols in the
821 Atmosphere. Science [J], 326(5959): 1525-1529.
822 Kalkavouras P, Bougiatioti A, Kalivitis N, et al. 2019. Regional new particle formation as modulators of
823 cloud condensation nuclei and cloud droplet number in the eastern Mediterranean. Atmos. Chem.
824 Phys. [J], 19(9): 6185-6203.
825 Kerminen V-M, Chen X, Vakkari V, et al. 2018. Atmospheric new particle formation and growth: Review
826 of field observations. Environmental Research Letters [J], 13(
827 Krechmer J E, Day D A, Ziemann P J, et al. 2017. Direct Measurements of Gas/Particle Partitioning and
828 Mass Accommodation Coefficients in Environmental Chambers. Environ Sci Technol [J],
829 51(20): 11867-11875.
830 Kulmala M, Dada L, Daellenbach K R, et al. 2021. Is reducing new particle formation a plausible solution
831 to mitigate particulate air pollution in Beijing and other Chinese megacities? Faraday
832 Discussions [J], 226(0): 334-347.
833 Kulmala M, L L, Lehtinen K, et al. 2004. Initial steps of aerosol growth. Atmospheric Chemistry and
834 Physics [J], 4(

Kulmala M, Petäjä T, Ehn M, et al. 2013. Chemistry of Atmospheric Nucleation: On the Recent Advances on Precursor Characterization and Atmospheric Cluster Composition in Connection with Atmospheric New Particle Formation. Annual review of physical chemistry [J], 65(

Kulmala M, Petäjä T, Nieminen T, et al. 2012. Measurement of the nucleation of atmospheric aerosol particles. Nature Protocols [J], 7(9): 1651-1667.

Lai S, Hai S, Gao Y, et al. 2022. The striking effect of vertical mixing in the planetary boundary layer on new particle formation in the Yangtze River Delta. Science of The Total Environment [J], 829(154607.

Lee S-H, Gordon H, Yu H, et al. 2019. New Particle Formation in the Atmosphere: From Molecular Clusters to Global Climate. Journal of Geophysical Research: Atmospheres [J], 124(

Li K, Zhu Y, Gao H, et al. 2015. A comparative study of cloud condensation nuclei measured between non-heating and heating periods at a suburb site of Qingdao in the North China. Atmospheric Environment [J], 112(40-53.

Li M, Liu H, Geng G, et al. 2017. Anthropogenic emission inventories in China: a review. National Science Review [J], 4(6): 834-866.

Li X, Li Y, Cai R, et al. 2022. Insufficient Condensable Organic Vapors Lead to Slow Growth of New Particles in an Urban Environment. Environmental Science & Technology [J], 56(14): 9936-9946.

Liu H J, Zhao C S, Nekat B, et al. 2014a. Aerosol hygroscopicity derived from size-segregated chemical composition and its parameterization in the North China Plain. Atmos. Chem. Phys. [J], 14(5): 2525-2539.

Liu M, Matsui H 2022. Secondary Organic Aerosol Formation Regulates Cloud Condensation Nuclei in the Global Remote Troposphere. Geophysical Research Letters [J], 49(18): e2022GL100543.

Liu X, Zhu Y, Zheng M, et al. 2014b. Production and growth of new particles during two cruise campaigns in the marginal seas of China. Atmospheric Chemistry and Physics [J], 14(

Liu X H, Zhu Y J, Zheng M, et al. 2014c. Production and growth of new particles during two cruise campaigns in the marginal seas of China. Atmos. Chem. Phys. [J], 14(15): 7941-7951.

Lovejoy E R, Curtius J, Froyd K D 2004. Atmospheric ion-induced nucleation of sulfuric acid and water. Journal of Geophysical Research: Atmospheres [J], 109(D8).

Lu H, Wang G, Guo H 2022. Ambient acidic ultrafine particles in different land-use areas in two representative Chinese cities. Science of The Total Environment [J], 830(154774.

Lu Y, Yan C, Fu Y, et al. 2019. A proxy for atmospheric daytime gaseous sulfuric acid concentration in urban Beijing. Atmos. Chem. Phys. [J], 19(3): 1971-1983.

Lupascu A, Easter R, Zaveri R, et al. 2015. Modeling particle nucleation and growth over northern California during the 2010 CARES campaign. Atmos. Chem. Phys. [J], 15(21): 12283-12313.

Ma N, Zhao C, Tao J, et al. 2016. Variation of CCN activity during new particle formation events in the North China Plain. Atmos. Chem. Phys. [J], 16(13): 8593-8607.

Matsui H, Koike M, Kondo Y, et al. 2011. Impact of new particle formation on the concentrations of aerosols and cloud condensation nuclei around Beijing. Journal of Geophysical Research: Atmospheres [J], 116(D19).

Matsui H, Koike M, Takegawa N, et al. 2013. Spatial and temporal variations of new particle formation in East Asia using an NPF-explicit WRF-chem model: North-south contrast in new particle formation frequency. 118(20): 11,647-611,663.

878 Merikanto J, Spracklen D V, Mann G W, et al. 2009. Impact of nucleation on global CCN. Atmos. Chem.
879 Phys. [J], 9(21): 8601-8616.
880 Mikkonen S, Romakkaniemi S, Smith J N, et al. 2011. A statistical proxy for sulphuric acid concentration.
881 Atmos. Chem. Phys. [J], 11(21): 11319-11334.
882 Morrison H, Thompson G, Tatarskii V 2009. Impact of Cloud Microphysics on the Development of
883 Trailing Stratiform Precipitation in a Simulated Squall Line: Comparison of One and Two-
884 Moment Schemes. Monthly Weather Review - MON WEATHER REV [J], 137(991-1007.
885 Napari I, Noppel M, Vehkamäki H, et al. 2002. Parametrization of ternary nucleation rates for H2SO4-
886 NH3-H2O vapors. Journal of Geophysical Research: Atmospheres [J], 107(D19): AAC 6-1-
887 AAC 6-6.
888 Nieminen T, Kerminen V M, Petäjä T, et al. 2018. Global analysis of continental boundary layer new
889 particle formation based on long-term measurements. Atmos. Chem. Phys. [J], 18(19): 14737-
890 14756.
891 Petäjä T, Mauldin I R L, Kosciuch E, et al. 2009. Sulfuric acid and OH concentrations in a boreal forest
892 site. Atmos. Chem. Phys. [J], 9(19): 7435-7448.
893 Pierce J, Riipinen I, Kulmala M, et al. 2011. Quantification of the volatility of secondary organic
894 compounds in ultrafine particles during nucleation events. Atmospheric Chemistry and Physics
895 Discussions [J], 11(14495-14539.
896 Pöschl U, Canagaratna M, Jayne J T, et al. 1998. Mass Accommodation Coefficient of H2SO4 Vapor on
897 Aqueous Sulfuric Acid Surfaces and Gaseous Diffusion Coefficient of H2SO4 in N2/H2O. The
898 Journal of Physical Chemistry A [J], 102(49): 10082-10089.
899 Qiao X, Yan C, Li X, et al. 2021. Contribution of Atmospheric Oxygenated Organic Compounds to
900 Particle Growth in an Urban Environment. Environmental Science & Technology [J], XXXX(
901 Ren J, Chen L, Fan T, et al. 2021. The NPF Effect on CCN Number Concentrations: A Review and Re-
902 Evaluation of Observations From 35 Sites Worldwide. Geophysical Research Letters [J], 48(19):
903 e2021GL095190.
904 Riipinen I, Sihto S L, Kulmala M, et al. 2007. Connections between atmospheric sulphuric acid and new
905 particle formation during QUEST III–IV campaigns in Heidelberg and Hyytiälä. Atmos.
906 Chem. Phys. [J], 7(8): 1899-1914.
907 Roldin P, Swietlicki E, Massling A, et al. 2011a. Aerosol ageing in an urban plume – implication for
908 climate. Atmos. Chem. Phys. [J], 11(12): 5897-5915.
909 Roldin P, Swietlicki E, Schurgers G, et al. 2011b. Development and evaluation of the aerosol dynamics
910 and gas phase chemistry model ADCHEM. Atmos. Chem. Phys. [J], 11(12): 5867-5896.
911 Saha S, Moorthi S, Wu X, et al. 2014. The NCEP Climate Forecast System Version 2. Journal of Climate
912 [J], 27(6): 2185-2208.
913 Shen X, Sun J, Zhang X, et al. 2018. Comparison of Submicron Particles at a Rural and an Urban Site in
914 the North China Plain during the December 2016 Heavy Pollution Episodes. Journal of
915 Meteorological Research [J], 32(26-37.
916 Shrivastava M, Fast J, Easter R, et al. 2011. Modeling organic aerosols in a megacity: comparison of
917 simple and complex representations of the volatility basis set approach. Atmospheric Chemistry
918 and Physics [J], 11(6639-6662.
919 Shrivastava M K, Lane T E, Donahue N M, et al. 2008. Effects of gas particle partitioning and aging of
920 primary emissions on urban and regional organic aerosol concentrations. 113(D18).

Sihto S L, Kulmala M, Kerminen V M, et al. 2006. Atmospheric sulphuric acid and aerosol formation: implications from atmospheric measurements for nucleation and early growth mechanisms. Atmos. Chem. Phys. [J], 6(12): 4079-4091.

Sihto S L, Mikkilä J, Vanhanen J, et al. 2011. Seasonal variation of CCN concentrations and aerosol activation properties in boreal forest. Atmos. Chem. Phys. [J], 11(24): 13269-13285.

Tewari M, Wang W, Dudhia J, et al. 2016. Implementation and verification of the united NOAH land surface model in the WRF model [M].

Virtanen A, Kannosto J, Kuuluvainen H, et al. 2011. Bounce behavior of freshly nucleated biogenic secondary organic aerosol particles. Atmos. Chem. Phys. [J], 11(16): 8759-8766.

Wang D-W, Guo H, Chan C K 2014. Diffusion Sampler for Measurement of Acidic Ultrafine Particles in the Atmosphere. Aerosol Science and Technology [J], 48(12): 1236-1246.

Wang J, Li M, Li L, et al. 2022. Particle number size distribution and new particle formation in Xiamen, the coastal city of Southeast China in wintertime. Science of The Total Environment [J], 826(154208.

Westervelt D M, Pierce J R, Riipinen I, et al. 2013. Formation and growth of nucleated particles into cloud condensation nuclei: model–measurement comparison. Atmos. Chem. Phys. [J], 13(15): 7645-7663.

Wu H, Li Z, Jiang M, et al. 2021a. Contributions of traffic emissions and new particle formation to the ultrafine particle size distribution in the megacity of Beijing. Atmospheric Environment [J], 262(118652.

Wu L, Ling Z, Shao M, et al. 2021b. Roles of Semivolatile/Intermediate-Volatility Organic Compounds on SOA Formation Over China During a Pollution Episode: Sensitivity Analysis and Implications for Future Studies. Journal of Geophysical Research: Atmospheres [J], 126(8): e2020JD033999.

Wu Z, Hu M, Yue D, et al. 2011. Evolution of particle number size distribution in an urban atmosphere during episodes of heavy pollution and new particle formation. Science China Earth Sciences [J], 54(11): 1772.

Yao L, Garmash O, Bianchi F, et al. 2018. Atmospheric new particle formation from sulfuric acid and amines in a Chinese megacity. Science [J], 361(278-281.

Yu F 2005. Quasi-unary homogeneous nucleation of H2SO4-H2O. The Journal of Chemical Physics [J], 122(7): 074501.

Yu F, Luo G, Nair A A, et al. 2020. Wintertime new particle formation and its contribution to cloud condensation nuclei in the Northeastern United States. Atmos. Chem. Phys. [J], 20(4): 2591-2601.

Yu F, Luo G, Pryor S C, et al. 2015. Spring and summer contrast in new particle formation over nine forest areas in North America. Atmos. Chem. Phys. [J], 15(24): 13993-14003.

Yuan Q, Li W, Zhou S, et al. 2015. Integrated evaluation of aerosols during haze-fog episodes at one regional background site in North China Plain. Atmospheric Research [J], 156(102-110.

Yue D L, Hu M, Zhang R Y, et al. 2011. Potential contribution of new particle formation to cloud condensation nuclei in Beijing. Atmospheric Environment [J], 45(33): 6070-6077.

Zaveri R A, Easter R C, Fast J D, et al. 2008. Model for Simulating Aerosol Interactions and Chemistry (MOSAIC). 113(D13).

Zaveri R A, Easter R C, Peters L K 2005. A computationally efficient Multicomponent Equilibrium Solver for Aerosols (MESA). Journal of Geophysical Research: Atmospheres [J], 110(D24).

965 Zhang Q, Jimenez J L, Canagaratna M R, et al. 2007. Ubiquity and dominance of oxygenated species in
966 organic aerosols in anthropogenically-influenced Northern Hemisphere midlatitudes.
967 Geophysical Research Letters [J], 34(13).
968 Zhao B, Wang S, Donahue N M, et al. 2016. Quantifying the effect of organic aerosol aging and
969 intermediate-volatility emissions on regional-scale aerosol pollution in China. Scientific
970 Reports [J], 6(1): 28815.
971 Zheng B, Tong D, Li M, et al. 2018. Trends in China's anthropogenic emissions since 2010 as the
972 consequence of clean air actions. Atmos. Chem. Phys. [J], 18(19): 14095-14111.
973 Zhu Y, Li K, Shen Y, et al. 2019. New particle formation in the marine atmosphere during seven cruise
974 campaigns. Atmos. Chem. Phys. [J], 19(1): 89-113.
975 Zhu Y, Sabaliauskas K, Liu X, et al. 2014. Comparative analysis of new particle formation events in less
976 and severely polluted urban atmosphere. Atmospheric Environment [J], 98(655-664.
977 Zhu Y, Shen Y, Li K, et al. 2021. Investigation of Particle Number Concentrations and New Particle
978 Formation With Largely Reduced Air Pollutant Emissions at a Coastal Semi-Urban Site in
979 Northern China. Journal of Geophysical Research: Atmospheres [J], 126(17): e2021JD035419.
980
981